

# Electrically switchable computer-generated hologram using a liquid crystal cell with a proton beam patterned polymethylmethacrylate substrate

D. Luo,<sup>1</sup> X. W. Sun,<sup>1,\*</sup> Y. J. Liu,<sup>1</sup> H. T. Dai,<sup>1</sup> O. Y. Sheng,<sup>2</sup>  
M. B. H. Breese,<sup>2,4</sup> and Z. Raszewski<sup>3</sup>

<sup>1</sup>School of Electrical and Electronic Engineering, Nanyang Technological University,  
Nanyang Avenue, Singapore 639798, Singapore

<sup>2</sup>CIBA, Department of Physics, National University of Singapore, 2 Science Drive 3, Singapore 117542, Singapore

<sup>3</sup>Institute of Applied Physics, Department of Advanced Technologies and Chemistry,  
Military University of Technology, 2 Kaliskiego St. Warsaw, Poland 00-908

<sup>4</sup>phymbhb@nus.edu.sg

\*Corresponding author: exwsun@ntu.edu.sg

Received 14 April 2009; accepted 8 June 2009;  
posted 11 June 2009 (Doc. ID 109670); published 24 June 2009

An electrically switchable computer-generated hologram (CGH) was fabricated using a liquid crystal (LC) cell. A polymethylmethacrylate (PMMA) film, which was spin-coated on one glass substrate of the LC cell, was patterned by a focused 2 MeV proton beam with a CGH phase pattern ( $2\ \mu\text{m}$  resolution). With an applied voltage on the LC cell CGH sample, an index modulation was produced between the regions with and without PMMA because of the reorientation of LC molecules under the external electric field. The maximum diffraction efficiency measured was about 28.7%. The operating voltage was below  $15\ \text{V}_{\text{rms}}$ . © 2009 Optical Society of America

OCIS codes: 050.1970, 230.3720, 090.1760.

## 1. Introduction

Computer-generated holograms (CGHs) are useful diffractive-optical elements for wave front manipulation [1], optical element testing [2], optical information processing [3,4], and three-dimensional display [5]. Various materials have been used to record CGH, such as photorefractive materials including BaTiO<sub>3</sub> crystal [6], Fe doped LiNbO<sub>3</sub> crystal [7], and even bacteriorhodopsin [8]. CGH devices based on liquid crystal (LC) spatial light modulators (SLMs) have also been reported [9–13].

Recently, we reported a switchable CGH using polymer-dispersed liquid crystals (PDLCs) [14,15] and a LC cell with patterned electrode [16]. The

phase shift can be obtained by reorientating the LC directors in a PDLC or LC cell when an external voltage is applied. In this paper, we report a CGH fabricated by a LC cell with a proton beam patterned polymethylmethacrylate (PMMA) substrate. This device has relatively low operating voltage ( $\sim 15\ \text{V}_{\text{rms}}$ ) and high resolution ( $\sim 2\ \mu\text{m}$ ), and it can be used as adaptive optical elements with a good electrically switchable property.

## 2. Experiment and Simulation

The phase distribution of the CGH was calculated by the conventional iterative Fourier transform algorithm [17]. The letters “NTU” were encoded into a CGH with  $128 \times 128$  binary-phase-only pixels. Figure 1(a) shows the phase distribution of the CGH, where the black and white regions represent a phase value of 0 and  $\pi$ , respectively. Figure 1(b) shows the

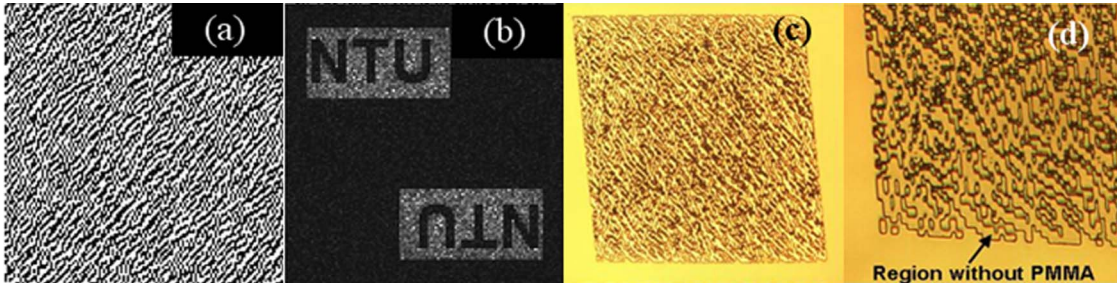


Fig. 1. (Color online) (a) Phase distributions of the CGH with “NTU” encoded, and (b) simulated reconstructed image of the CGH, and optical microscopic images of PMMA with CGH phase pattern encoded by a proton beam with (c) low (10 $\times$ ) and (d) high (20 $\times$ ) magnifications.

simulated reconstructed image of the CGH. A focused 2 MeV proton beam was used to write the phase distribution of the CGH directly into a 5  $\mu\text{m}$  thick PMMA film [18,19], which was spin-coated on an indium tin oxide (ITO)-coated glass substrate. The CGH was patterned in an effective area of 2 mm  $\times$  2 mm containing 1024  $\times$  1024 pixels (2  $\mu\text{m}$  resolution). Figures 1(c) and 1(d) show the morphologies of the CGH on PMMA film observed from an optical microscope with low (10 $\times$ ) and high (20 $\times$ ) magnifications, respectively. The region without PMMA is marked in Fig. 1(d).

The ITO glass with proton beam patterned PMMA was then used to assemble a LC cell with a normal ITO glass. The inner surface of this counter ITO glass substrate without PMMA was coated with a polyimide layer and rubbed. Then the LC cell was filled with the E7 LC (from Merck, with an ordinary refractive index of  $n_o = 1.5216$  and birefringence of  $\Delta n = 0.2248$ ). LC molecules are aligned in the rubbing direction and cell gap  $d$  is 16.5  $\mu\text{m}$ .

Figure 2 shows the schematic cross section of the LC CGH sample. For normal incident light, the relative phase difference ( $\Delta\delta$ ) between the regions with and without PMMA can be written as

$$\Delta\delta = \frac{2\pi}{\lambda} [(n_{\text{eff}1}(d+h) - (n_{\text{eff}2} \cdot d + n_p \cdot h)], \quad (1)$$

where  $d$  is the cell gap (16.5  $\mu\text{m}$ ),  $h$  is the thickness of PMMA film (5  $\mu\text{m}$ ),  $\lambda$  is the wavelength,  $n_p = 1.49$  is the PMMA refractive index, and  $n_{\text{eff}1}$  and  $n_{\text{eff}2}$  are the effective LC refractive indices in the region without and with PMMA, respectively. The detailed experimental setup of image reconstruction from the

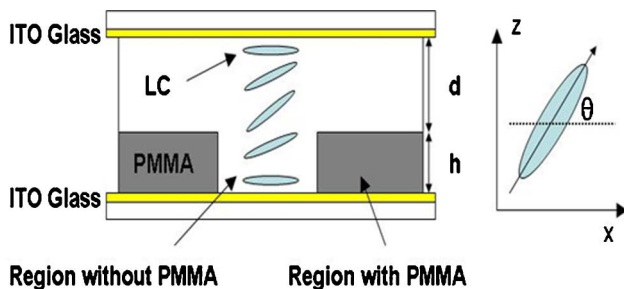


Fig. 2. (Color online) Schematic cross section of a LC cell with one PMMA pattern glass.

LC cell CGH sample can be found elsewhere [14]. In this experiment, the polarization of incident light was parallel to the rubbing direction of the cell.

It is necessary to point out that, because the PMMA substrate is not rubbed, the actual LC orientation on this substrate, where the anchoring is more complicated in contrast to the other substrate with rubbing, is not uniform and could be affected by the PMMA walls. This nonuniform orientation of the LC was observed by checking the CGH sample under an optical microscope through two cross polarizers with rubbing direction of the cell parallel to the optical axis of one polarizer. Moreover, the sharp edges of the PMMA CGH pattern could result in local dislocations or defects. Because of the irregular pattern of the CGH, at present, it is not possible to consider all these factors in our simulation to determine the phase change as a function of voltage. Thus, in the following model, we assume a homogenous alignment assumption (antiparallel rubbing). Though there is some discrepancy between the simulation and experiment (Fig. 4), our model is still able to match the experiment well.

When applied voltage is added on the LC cell, LC molecules are forced to align along the direction of the electric field in the cell. Following the Oseen–Frank theory, the elastic energy density ( $U_{\text{EL}}$ ) of a deformed LC can be written by

$$U_{\text{EL}} = \frac{1}{2}K_{11}(\nabla \cdot \mathbf{n})^2 + \frac{1}{2}K_{22}(\mathbf{n} \cdot \nabla \times \mathbf{n})^2 + \frac{1}{2}K_{33}(\mathbf{n} \times \nabla \times \mathbf{n})^2, \quad (2)$$

where  $\mathbf{n}$  is a unit vector representing the LC molecule director in the cell, and  $K_{11}$ ,  $K_{22}$ , and  $K_{33}$  are the splay, twist, and bend elastic constants, respectively.

In this paper, we chose a homogeneous alignment configuration to numerically model the LC electro-optics effect, and the molecule director is

$$\mathbf{n} = (\cos \theta, 0, \sin \theta), \quad (3)$$

where  $\theta$  is the orientation angle between the director and the  $x$  axis (shown in Fig. 2). The total free energy ( $U$ ) including elastic energy and electromagnetic energy in the cell can be given by

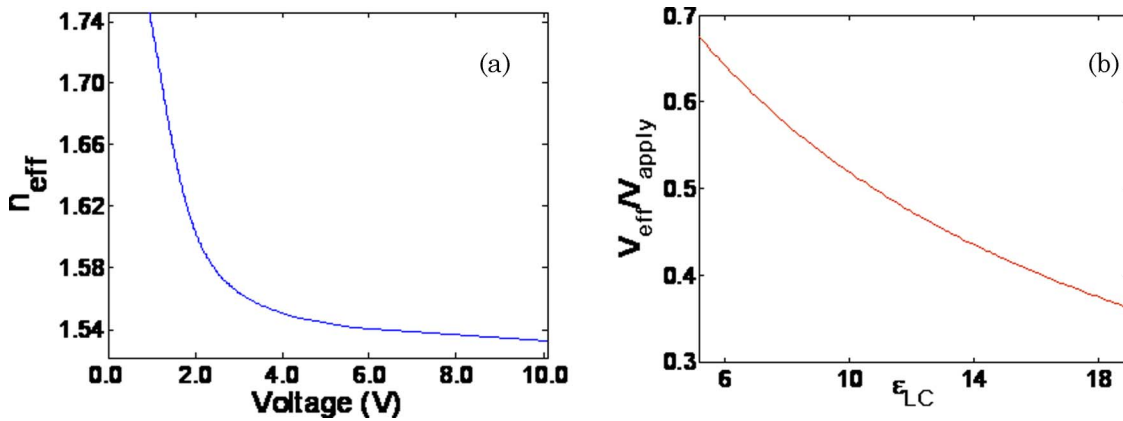


Fig. 3. (Color online) (a) Relationship between the effective refractive index and the applied voltage for homogeneous alignment configuration. (b) Relationship of  $V_{\text{eff}}/V_{\text{apply}}$  and  $\epsilon_{\text{LC}}$  with  $h = 5 \mu\text{m}$  and  $d = 16.5 \mu\text{m}$ .

$$U = \int_0^L \left[ \frac{1}{2} (K_{11} \cos^2 \theta + K_{33} \sin^2 \theta) \left( \frac{d\theta}{dz} \right)^2 + \frac{1}{2\epsilon_0} \frac{D_z^2}{(\epsilon_{\parallel} \sin^2 \theta + \epsilon_{\perp} \cos^2 \theta)} - \frac{1}{2\epsilon_0} \frac{D_z^2}{\epsilon_{\perp}} \right] dz, \quad (4)$$

$$\begin{aligned} & (K_{11} \cos^2 \theta + K_{33} \sin^2 \theta) \left( \frac{d\theta}{dz} \right)^2 \\ &= \frac{D_z^2}{\epsilon_0 (\epsilon_{\parallel} \sin^2 \theta + \epsilon_{\perp} \cos^2 \theta)} - \frac{D_z^2}{\epsilon_0 (\epsilon_{\parallel} \sin^2 \theta_m + \epsilon_{\perp} \cos^2 \theta_m)}, \end{aligned} \quad (5)$$

where  $L$  is the thickness of the LC cell in  $z$  direction,  $D_z$  ( $=$  constant) is the  $z$  component of the electric displacement field vector,  $\epsilon_0$  is the dielectric constant in free space, and  $\epsilon_{\parallel}$  and  $\epsilon_{\perp}$  are the dielectric constants of parallel and perpendicular to the molecule director of the nematic LC, respectively. The LC molecule director distribution will be in the equilibrium state where the total free energy is minimized. Using techniques of calculus of variation, we obtain

where  $\theta_m$  is the maximum orientation angle at the center of the cell  $z = L/2$ . Here we assumed strong anchoring at both surfaces, which means the directors at the boundaries remain parallel to the rubbed direction ( $\theta(0) = \theta(L) = 0$ ). The molecule director distribution inside the cell  $\theta(z)$  can be calculated at a given applied voltage by numerically solving Eq. (5).

When the polarization direction of incident light is parallel to the rubbed direction, light in the LC cell will experience extraordinary refractive index. Correspondingly, the distribution of extraordinary refractive index in the LC cell and the effective refractive index can be simplified by a one-dimensional solution

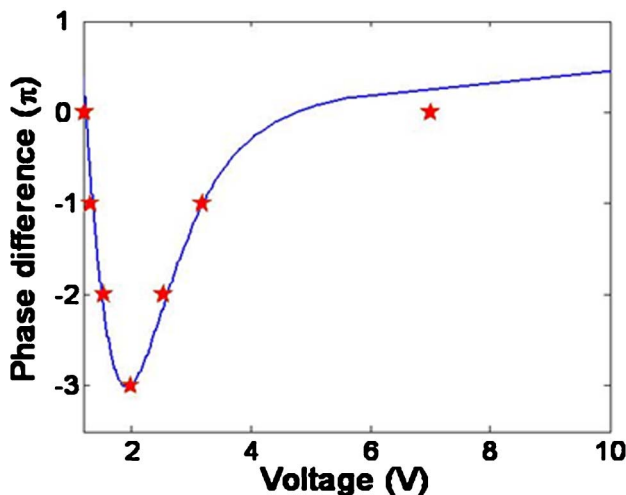


Fig. 4. (Color online) Solid blue line shows the theoretical relationship of phase difference and applied voltage, and red stars represent the experimental phase difference at applied voltage of 1.2, 1.32, 1.54, 1.97, 2.53, 3.18, and  $7.0 V_{\text{rms}}$ , respectively.

$$n_{\text{eff}} = \frac{1}{L} \int_0^L \frac{n_o n_e}{(n_o^2 \cos^2 \theta_z + n_e^2 \sin^2 \theta_z)^{1/2}} dz, \quad (6)$$

where  $n_o$  and  $n_e$  are the ordinary and the extraordinary refractive index of LC, respectively.

The LC we used was E7 from Merck with  $n_o = 1.5216$  and  $n_e = 1.7462$ . The dielectric constants of E7 are  $\epsilon_{\parallel} = 19.0$  and  $\epsilon_{\perp} = 5.2$ , at 1 kHz frequency and room temperature. The splay and bend elastic constants of E7 chosen here are  $K_{11} = 11.01 \times 10^{-12} \text{N}$  and  $K_{33} = 17.01 \times 10^{-12} \text{N}$ , respectively. Figure 3(a) shows the simulated relationship between the effective refractive index and the applied voltage. The calculated theoretical threshold voltage is about  $0.94 V_{\text{rms}}$ .

When voltage is applied on the region with the PMMA of our device, the effective voltage on the LC will be reduced because the PMMA is an insulator

(with a dielectric constant of approximately  $\epsilon_p = 3$  [20]). From the boundary condition on the electric field of Maxwell's equations, in the region with PMMA, we can obtain

$$\mathbf{D}_{\text{LC}_n} - \mathbf{D}_{\text{PMMA}_n} = \sigma_f = 0, \quad (7)$$

where  $\mathbf{D}_{\text{LC}_n}$  and  $\mathbf{D}_{\text{PMMA}_n}$  are the normal component of electric displacement of LC and PMMA materials respectively, and  $\sigma_f$  is the free surface charge density (equal to zero here). According to Eq. (7), the effective voltage distributed on the LC part ( $V_{\text{eff}}$ ) in the region with PMMA can be determined by solving

$$V_{\text{eff}} = \frac{1}{1 + \frac{\epsilon_{\text{LC}} \cdot h}{\epsilon_p \cdot d}} V_{\text{apply}}, \quad (8)$$

where  $V_{\text{apply}}$  is the external applied voltage on the two ITO layers and  $\epsilon_{\text{LC}}$  is the effective dielectric constant of LC at the interface of PMMA and LC in the region with PMMA. The relationship of  $V_{\text{eff}}/V_{\text{apply}}$  and  $\epsilon_{\text{LC}}$  is shown as Fig. 3(b), from which we can see that the ratio of  $V_{\text{eff}}$  to  $V_{\text{apply}}$  decreases with the increase of  $\epsilon_{\text{LC}}$ .

### 3. Results and Discussions

Given  $V_{\text{apply}}$ , we can determine  $V_{\text{eff}}$ ,  $n_{\text{eff}1}$ , and  $n_{\text{eff}2}$ . Hence, the corresponding phase difference can be determined using Eq. (1). For  $\epsilon_{\text{LC}} = \epsilon_{\perp} = 5.2$ , we calculated that around 67.5% of the external applied voltage is finally applied on the LC for  $h = 5 \mu\text{m}$  and  $d = 16.5 \mu\text{m}$ .

Under applied voltage, the reconstructed image would become blurred if the phase difference is the even integer times of  $\pi$  and the reconstructed image would become clear if the phase difference is the odd integer times of  $\pi$ . In our experiments, the blurred images were found at a voltage of 1.2, 1.54, 2.53, and  $7.0 V_{\text{rms}}$ , corresponding to  $0\pi$ ,  $-2\pi$ ,  $-2\pi$ , and  $0\pi$ , respectively. The clear images were observed at voltage of 1.32, 1.97, and  $3.18 V_{\text{rms}}$ , corresponding to  $-\pi$ ,  $-3\pi$ , and  $-\pi$ , respectively. In Fig. 4, the solid blue line shows the theoretical relationship of the phase difference and applied voltage, and the red stars represent the experimental phase difference at an applied voltage of 1.2, 1.32, 1.54, 1.97, 2.53, 3.18, and  $7.0 V_{\text{rms}}$ , respectively. We can see that the experimental data are consistent with the calculated results. In our experiment, the image started to change from  $1.2 V_{\text{rms}}$ , i.e., the experimental threshold was about  $1.2 V_{\text{rms}}$ .

Figures 5(a) and 5(b) show the reconstructed images of the LC cell CGH sample with an applied voltage of 1.9 and  $12 V_{\text{rms}}$ , respectively. To reduce the scattered light from the brightest zeroth-order beam in the reconstructed image, a hole was drilled in the middle of the image screen. As the applied voltage exceeds the threshold ( $1.2 V_{\text{rms}}$ ), the images change between blurred and clear alternately several times. The blurred image is primarily due

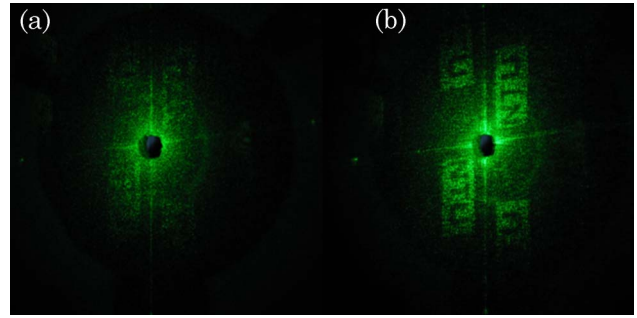


Fig. 5. (Color online) Reconstructed images of the LC cell CGH sample with an applied voltage of (a)  $1.54 V_{\text{rms}}$ , and (b)  $12 V_{\text{rms}}$ , respectively.

to phase mismatch, originated from nonuniform anchoring on the PMMA walls and sharp edges, leading to poor/nonuniform modulation. Also the small PMMA wall spacing could generate strong anchoring LC forces leading to poor modulation capability. It is noticed that the image at higher voltage (e.g.,  $12 V_{\text{rms}}$ ) is clearer than those at lower voltages (e.g., 1.32, 1.97, and  $3.18 V_{\text{rms}}$ ). This poor quality at lower voltage probably results from a poor phase modulation and error due to complex LC orientation related to the CGH pattern. In contrast, at a higher voltage, the LC directors will reorient mostly along the applied electric field and become more ordered, resulting in reduced light scattering and hence a clearer reconstructed image. For higher applied voltages ( $>12 V_{\text{rms}}$ ), there is no further change in the reconstructed image, indicating that the LC molecules are strictly perpendicular to the substrate. The calculated phase difference stays at around  $0.57\pi$  for voltages higher than  $12 V_{\text{rms}}$ . The diffraction efficiency is defined by the ratio of the light intensity of the first order diffraction to the total transmitted light intensity through the CGH in the reconstructed image plane, which can be measured directly. The maximum diffraction efficiency measured was about 28.7% at  $12 V_{\text{rms}}$ , less than the theoretical maximum binary phase first order diffraction efficiency of 41% [21]. We had checked the CGH sample under an optical microscope through cross polarizers with no voltage applied. The direction of LC molecules in the region without PMMA were not exactly along the rubbing direction, which will reduce the initial phase difference between the regions with and without PMMA, leading to  $n_{\text{eff}}$  differences between the theoretical and the experimental  $n_{\text{eff}}$  values under applied voltages.

Although the polarization of the incident light chosen in our experiment was parallel to the rubbing direction of the LC cell, i.e., an effective extraordinary refractive index of LC was experienced by the incident light, the reconstructed image of the CGH can also be obtained by using incident light with polarization perpendicular to the rubbing direction of the LC cell, since the ordinary refractive index of LC ( $n_o = 1.521$ ) and the refraction index of PMMA ( $n_p = 1.49$ ) are not equal. In this configuration, the relative

phase difference  $\Delta\delta$  was calculated to be  $0.57\pi$ . With an applied external voltage, the relative phase difference and the reconstructed image of the CGH kept unchanged.

The electro-optical response of the LC cell CGH sample was measured by switching the applied voltage between 4.5 and  $24V_{\text{rms}}$  with a frequency of 2.6 Hz. The rising time and falling time are about 62 and 60 ms, respectively. This response time is slower than that of a CGH device fabricated by PDLC [14]. Reducing the LC cell gap would lead to a faster response time.

The advantages of proton beam writing used in this paper are that it has a deep penetration in resist materials with little lateral scattering, which enables proton beam writing to fabricate high aspect-ratio microstructures with vertical, smooth sidewalls and low line edge roughness. The highest resolution achieved is around 50 nm and a 2 MeV proton will penetrate about  $60\mu\text{m}$  into PMMA. The high aspect ratio could be used to fabricate a Bragg diffraction volume grating with a high diffracting efficiency. Compared to the CGH recorded in the PDLC where a transparency mask was used with a resolution of  $50\mu\text{m}$  in our previous work [14], a higher resolution ( $\sim 2\mu\text{m}$ ) was achieved by the proton beam in this paper, leading to better quality of the reconstructed CGH image. It has less light scattering and relatively lower operating voltage ( $\sim 15V_{\text{rms}}$ ), compared to a CGH using PDLC material [14]. Higher cost and longer fabricate time are the drawbacks of this method.

#### 4. Conclusion

In conclusion, we demonstrated an electrically switchable CGH using a LC cell with proton beam patterned PMMA film. It has a relatively low operating voltage ( $\sim 15V_{\text{rms}}$ ) and a high resolution ( $\sim 2\mu\text{m}$ ). The maximum diffraction efficiency measured is about 28.7%. This device is promising in adaptive optical elements.

This work was supported by a Poland–Singapore collaborative project sponsored by the Agency for Science, Technology and Research of Singapore (No. 062 120 0016) and the Ministry and Science and Technology of Poland (No. SINGAPUR 13/2006).

#### References

1. W. H. Lee, "Computer generated holograms: techniques and applications," in *Progress in Optics*, E. Wolf, ed. (Elsevier Science, 1978), Vol XVI, pp. 119–232
2. A. J. MacGovern and J. C. Wyant, "Computer generated holograms for testing optical element," *Appl. Opt.* **10**, 619–624 (1971).
3. A. W. Lohman and J. C. Wyant, "Binary Fraunhofer holograms generated by computer," *Appl. Opt.* **6**, 1739–1748 (1967).

4. D. Casasent and C. Szczutkowski, "Optical Mellin transforms using computer generated holograms," *Opt. Commun.* **19**, 217–222 (1976).
5. W. J. Dallas, "Computer-generated holograms," in *The Computer in Optical Research: Methods and Applications*, B. R. Frieden, ed, Vol. 41 of Topics in Applied Physics (Springer-Verlag, 1980), pp. 291–366.
6. L. Pugliese and G. M. Morris, "Computer-generated holography in photorefractive materials," *Opt. Lett.* **15**, 338–340 (1990).
7. K. Nakagawa, S. Iguchi, and T. Minemoto, "Computer-generated holograms in photorefractive LiNbO<sub>3</sub> crystal," *Proc. SPIE* **3470**, 77–83 (1998).
8. F. Guessous, T. Juchem, and N. Hampp, "Computer generated holograms recorded in bacteriorhodopsin," *Proc. SPIE* **5310**, 369–376 (2004).
9. F. Mok, J. Diep, H. K. Liu, and D. Psaltis, "Real-time computer-generated hologram by means of liquid-crystal television spatial light modulator," *Opt. Lett.* **11**, 748–750 (1986).
10. C. S. Guo, Z. Y. Rong, H. T. Wang, Y. R. Wang, and L. Z. Cai, "Phase-shifting with computer-generated holograms written on a spatial light modulator," *Appl. Opt.* **42**, 6975–6979 (2003).
11. V. Arrizon, L. A. Gonzalez, R. Ponce, and A. Serrano-Heredia, "Computer-generated holograms with optimum bandwidths obtained with twisted-nematic liquid-crystal displays," *Appl. Opt.* **44**, 1625–1634 (2005).
12. S. Chavali, P. M. Birch, R. Young, and C. Chatwin, "Synthesis and reconstruction of computer generated holograms by a double pass technique on a twisted nematic-based liquid crystal spatial light modulator," *Opt. Lasers Eng.* **45**, 413–418 (2007).
13. G. Zito, B. Piccirillo, E. Santamato, A. Marino, V. Tkachenko, and G. Abbate, "Two-dimensional photonic quasicrystals by single beam computer-generated holography," *Opt. Express* **16**, 5164–5170 (2008).
14. Y. J. Liu and X. W. Sun, "Electrically switchable computer-generated hologram recorded in polymer-dispersed liquid crystals," *Appl. Phys. Lett.* **90**, 191118 (2007).
15. Y. J. Liu, X. W. Sun, Q. Wang, and D. Luo, "Electrically switchable optical vortex generated by a computer-generated hologram recorded in polymer-dispersed liquid crystals," *Opt. Express* **15**, 16645–16650 (2007).
16. Y. J. Liu, X. W. Sun, D. Luo, and Z. Raszewski, "Generating electrically tunable optical vortices by a liquid crystal cell with patterned electrode," *Appl. Phys. Lett.* **92**, 101114 (2008).
17. R. W. Gerchberg and W. O. Saxton, "A practical algorithm for the determination of phase from image and diffraction plane pictures," *Optik (Stuttg.)* **35**, 237 (1972).
18. M. B. H. Breese, G. W. Grime, and F. Watt, "MeV ion beam lithography of PMMA," *Nucl. Instrum. Methods Phys. Res. B* **77**, 169–174 (1993).
19. F. Watt, J. A. van Kan, I. Rajta, A. A. Bettiol, T. F. Choo, M. B. H. Breese, and T. Osipowicz, "The National University of Singapore high energy ion nano-probe facility: performance tests," *Nucl. Instrum. Methods Phys. Res. B* **210**, 14–20 (2003).
20. Z. Z. Zhong, D. E. Schuele, W. L. Gordon, K. J. Adamic, and R. B. Akins, "Dielectric properties of a PMMA/E7 polymer-dispersed liquid crystal," *J. Polym. Sci. Polym. Phys.* **30**, 1443–1449 (1992).
21. J. A. Cox, T. Werner, J. Lee, S. Nelson, B. Fritz, and J. Bergstrom, "Diffraction efficiency of binary optical elements," *Proc. SPIE* **1211**, 116–124 (1990).